Clim Dyn (2013) 41:1067–1081
DOI 10.1007/s00382-013-1859-9

Multi-model MJO forecasting during DYNAMO/CINDY period

Xiouhua Fu · June-Yi Lee · Pang-Chi Hsu · Hiroshi Taniguchi · Bin Wang · Wanqiu Wang · Scott Weaver

Received: 1 January 2013 / Accepted: 24 June 2013 / Published online: 14 July 2013

Abstract The present study assesses the forecast skill of the Madden–Julian Oscillation (MJO) observed during the period of DYNAMO (Dynamics of the MJO)/CINDY (Cooperative Indian Ocean Experiment on Intraseasonal Variability in Year 2011) field campaign in the GFS (NCEP Global Forecast System), CFSv2 (NCEP Climate Forecast System version 2) and UH (University of Hawaii) models, and revealed their strength and weakness in forecasting initiation and propagation of the MJO. Overall, the models forecast better the successive MJO which follows the preceding event than that with no preceding event (primary MJO). The common modeling problems include too slow eastward propagation, the Maritime Continent barrier and weak intensity. The forecasting skills of MJO major modes reach 13, 25 and 28 days, respectively, in the GFS atmosphere-only model, the CFSv2 and UH coupled models. An equal-weighted multi-model ensemble with the CFSv2 and UH models reaches 36 days. Air–sea coupling plays an important role for initiation and propagation of the MJO and largely accounts for the skill difference between the GFS and CFSv2. A series of forecasting experiments by forcing UH model with persistent, forecasted and observed daily SST further demonstrate that: (1) air–sea coupling extends MJO skill by about 1 week; (2) atmosphere-only forecasts driven by forecasted daily SST have a similar skill as the coupled forecasts, which suggests that *if the high-resolution GFS is forced with CFSv2 forecasted daily SST, its forecast skill can be much higher than its current level as forced with persistent SST*; (3) atmosphere-only forecasts driven by observed daily SST reaches beyond 40 days. It is also found that the MJO–TC (Tropical Cyclone) interactions have been much better represented in the UH and CFSv2 models than that in the GFS model. Both the CFSv2 and UH coupled models reasonably well capture the development of westerly wind bursts associated with November 2011 MJO and the cyclogenesis of TC05A in the Indian Ocean with a lead time of 2 weeks. However, the high-resolution GFS atmosphere-only model fails to reproduce the November MJO and the genesis of TC05A at 2 weeks' lead. This result highlights the necessity to get MJO right in order to ensure skillful extended-range TC forecasting.

Keywords MJO forecasting skill · GFS, CFSv2, and UH global models · DYNAMO/CINDY field campaign · Air–sea coupling · Atmosphere-only forecast · MJO–TC interactions · Extended-range TC forecasting

This paper is a contribution to the Topical Collection on Climate Forecast System Version 2 (CFSv2). CFSv2 is a coupled global climate model and was implemented by National Centers for Environmental Prediction (NCEP) in seasonal forecasting operations in March 2011. This Topical Collection is coordinated by Jin Huang, Arun Kumar, Jim Kinter and Annarita Mariotti.

X. Fu (✉) · J.-Y. Lee · P.-C. Hsu · H. Taniguchi · B. Wang
International Pacific Research Center (IPRC), SOEST,
University of Hawaii at Manoa, 1680 East West Road,
POST Bldg. 409D, Honolulu, HI 96822, USA
e-mail: xfu@hawaii.edu

W. Wang · S. Weaver
Climate Prediction Center, NOAA/NWS/NCEP,
College Park, MD, USA

1 Introduction

The Madden–Julian Oscillation (MJO) is the dominant mode of tropical convection variability on the intraseasonal timescales (Madden and Julian 1971; Zhang 2005; Lau and Waliser 2011). The MJO convective envelope initiates over

the equatorial Africa and western equatorial Indian Ocean (Wang and Rui 1990a). The associated circulation systems propagate eastward as a Kelvin–Rossby wave couplet (Wang and Rui 1990b; Hendon and Salby 1994; Roundy 2012) involving multi-scale interactions (Majda and Biello 2004; Wang and Liu 2011). On its way eastward, the MJO modulates tropical cyclone (TC) activity over the Indian Ocean (Kikuchi et al. 2009; Fu and Hsu 2011), western Pacific (Liebmann et al. 1994; Nakazawa 2006), Eastern North Pacific, and Atlantic basin (Molinari et al. 1997; Maloney and Hartmann 2000; Mo 2000; Higgins and Shi 2001; Klotzbach 2010). Through upscale/downscale modulations and tropical-extratropical tele-connection, the MJO also influences global weather and climate variability (Donald et al. 2006). The recurrent nature of the MJO with a period of 30–60 days offers an opportunity to bridge the forecasting gap between medium-range weather forecast ($\sim$1 week) and seasonal prediction (longer than 1 month) (e.g., Waliser 2006; Fu et al. 2008; Brunet et al. 2010; Hoskins 2012). Most global operational and research weather/climate models, however, still face a variety of challenges to realistically simulate and accurately predict the MJO (Lin et al. 2006; Vitart et al. 2007; Wang and Seo 2009; Gottschalck et al. 2010; Rashid et al. 2010; Fu et al. 2011; Weaver et al. 2011; and Matsueda and Endo 2011), therefore, severely hindering the extended-range TC forecasting (Belanger et al. 2012; Fu 2012) and the prediction of MJO's global impacts (Vitart and Molteni 2010).

In order to provide a ground truth for the purposes of better understanding of the physical processes governing the initiation and propagation of the MJO and evaluating and improving its representations in operational and research weather/climate models, a comprehensive international collaborative field campaign (DYNAMO/CINDY)[1] has been launched over western-central equatorial Indian Ocean from October 1st, 2011 to March 31st, 2012 with an Intensive Observing Period (IOP) from October 1st, 2011 to January 15th, 2012. During the entire DYNAMO period, five MJO events are observed (Fig. 1) with associated convective envelope over Indian Ocean, respectively, in the late October (MJO-I), late November (MJO-II), late December (MJO-III), late January (MJO-IV), and late February-early March (MJO-V). The first three MJOs occur during DYNAMO IOP. The definition of MJO initiation is still a controversial issue (e.g., Straub 2013) and Indian Ocean is also not the only place for MJO initiation (Wang and Rui 1990a; Matthews 2008). Nevertheless, following the classical schematics of a MJO cycle depicted in Fig. 16 of Madden and Julian (1972), we take the definition of MJO initiation as the onset of convective envelope in the Indian Ocean associated with an eastward-propagating MJO event. The MJOs-I, II, and V are clearly successive MJO events as defined by Matthews (2008), which are re-initiated over Indian Ocean by the circum-global circulations associated with a preceding MJO event. In 2011 summer (JJA), no apparent MJO events were observed. The MJO-I was likely initiated by a primary MJO developed in late September over the western Pacific just before the start of the DYNAMO/CINDY IOP. In a similar fashion, the MJO-II was initiated by the circum-global circulations of the MJO-I. The westerly wind bursts of November MJO-II reached DYNAMO array around November 23rd, which triggered the development of a near-equatorial tropical cyclone (also known as Thanks-giving-TC in DYNAMO community[2]). The MJO-III is not well defined and also the weakest among the five MJOs. The MJO-III, initiated over central Indian Ocean, was likely triggered by the westward-propagating mixed-Rossby-gravity waves emanated from the Maritime Continent, which in turn were excited by the remnants of a tropical cyclone in the South China Sea (Kubota et al. 2012). In the month of December 2011, a La Nina event matured in the equatorial eastern and central Pacific Ocean and extended westward to 160°E. The resultant cold SST near the deadline suppresses the continuous eastward propagations of the convection of the MJO and Kelvin waves (Fig. 1). The decayed eastward-propagating convection, instead, emanates westward-propagating equatorial Rossby waves (Wang and Xie 1997). From January to March of 2012, the La Nina event quickly decays and transitions into an above-normal status. At the same time, SST annual cycle keeps warm up the equatorial Pacific. Along with the gradual warming of the equatorial Pacific, a weak MJO-IV develops, followed by a huge MJO-V with its convective envelope moving slowly from Indian Ocean to western Pacific during the late February and March (Fig. 1). Due to the political unrest of Maldives, all DYNAMO/CINDY in situ observing instruments were moved out after early February 2012 considering the safety of all field-campaign participants. Therefore, no intensive in situ observations are available for the big MJO-V.

Since the late August 2011, NCEP CPC has been preparing a MJO-discussion-summary[3] for DYNAMO/CINDY field campaign each week that assembled two-week-lead forecasts from at least seven operational centers. After carefully reviewing all forecasts from September 1st,

[1] More details on the DYNAMO and CINDY field campaigns can be found at: http://www.eol.ucar.edu/projects/dynamo/ and http://www.jamstec.go.jp/iorgc/cindy/.

[2] Fishermen died unnecessarily in Tropical Cyclone-TC05A: http://maddenjulianconversation.blogspot.com/2011/11/fishermen-died-unnecessarily-in.html.

[3] All real-time forecasts and discussions are available online: http://catalog1.eol.ucar.edu/cgi-bin/dynamo/report/index).

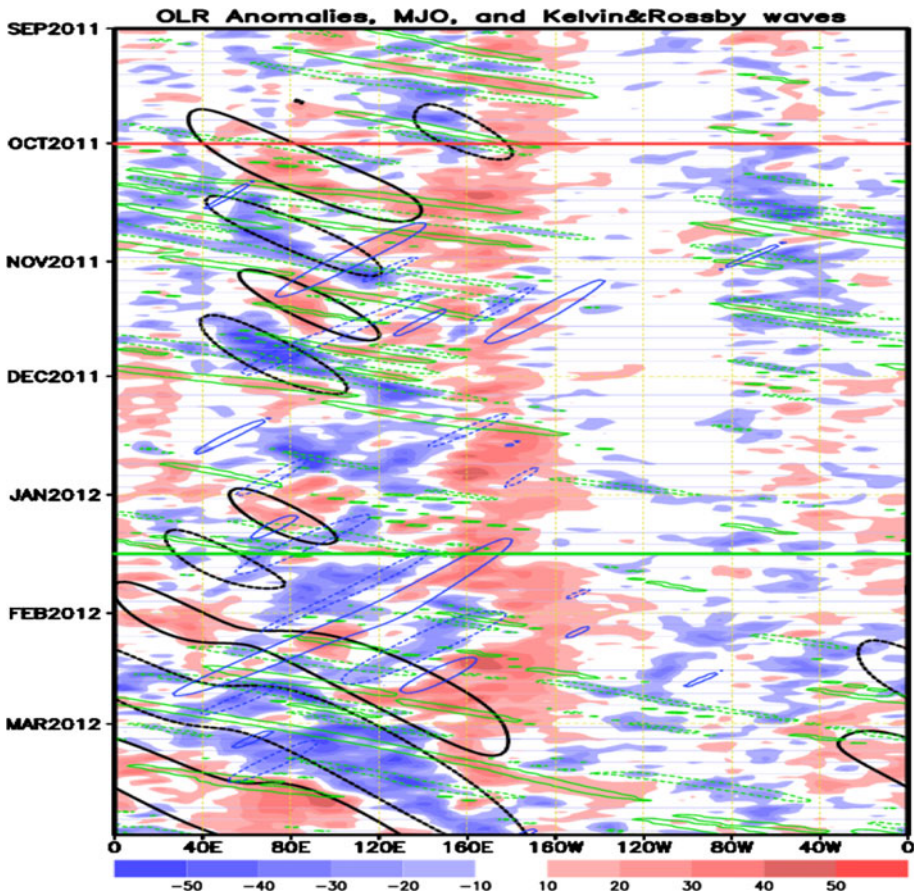

Fig. 1 Hovemoller diagram of observed OLR anomalies averaged between 10°S and 10°N (*Shading*, unit: W m^{-2}) along with MJO (*black contours*), Kelvin (*green contours*) and Rossby waves (*blue contours*) during DYNAMO/CINDY period (only −10 and 10 W m^{-2} *lines* are drawn). The method used to extract the MJO and equatorial waves is after Wheeler and Hendon (2004)

2011 to March 31st, 2012, we have highlighted the major strength and weakness of these operational forecasts in a supplementary material.[4] Current operational intraseasonal forecasting systems have higher skill for the successive MJOs-I, II, and V than that for the primary MJO in September and the MJOs-III and IV. During the entire DYNAMO/CINDY period, the common problems of operational models on MJO forecasts are: (1) the failure to predict the September primary MJO even with 1 week lead; (2) too slow eastward propagation; (3) the Maritime Continent barrier; (4) the difficulty to predict the MJO initiated by Rossby (or mixed-Rossby-gravity) waves; and (5) the underestimation of the observed intensity.

This study aims to: (1) quantify the MJO forecasting skills of NCEP operational models and UH (University of Hawaii) research model during DYNAMO/CINDY period; (2) reveal the strength and weakness of the models on forecasting initiation and propagation of the MJO; (3) assess the impacts of air–sea coupling on MJO forecasting and possible consequence on extended-range TC forecasting. The outline of this paper is as follows. In Sect. 2, we briefly introduce the three state-of-the-art global models: the NCEP GFS (Global Forecast System) atmosphere-only model, CFSv2 (Climate Forecast System version 2) and UH coupled models, along with the data and methodology used in this study. Section 3 documents the overall MJO forecasting skills during the entire DYNAMO/CINDY period and that just during the IOP in three models and highlights the strength and weakness of individual models in forecasting the initiation and propagation of the MJO. In Sect. 4, the impacts of air–sea coupling, forced with persistent, forecasted and observed daily SST on MJO forecasting skills are assessed through a series of forecasting experiments using UH model. Section 5 examines three models' capability in representing the interactions of November-MJO and Thanksgiving-TC and potential impacts on extended-range TC forecasting in these models. Discussions and concluding remarks are given in Sect. 6.

2 Models and methodology

This study analyzes forecasts from three models: The Global Forecast System (GFS), the Climate Forecast System version 2 (CFSv2), and the University of Hawaii (UH) model. The GFS used to generate forecasts for the DYNAMO/CINDY period is the NCEP operational 2-week

[4] This material is available online: http://www.soest.hawaii.edu/~xfu/dynamo_op_fcst.pdf.

atmosphere-only forecasting system. The horizontal resolution is T574 (~27 km) for the first week and reduces to T190 (~70 km) for the second week. This system is initialized with the NCEP Global Data Assimilation System (GDAS). The forecasts are driven by the observed climatological SST plus initial SST anomaly that decays with lead time at an e-folding time scale of 90 days. This setting results in a basically persistent SST forcing during the 2-week forecast period. Daily four-time (00Z, 06Z, 12Z and 18Z) forecasts are treated as 4 ensemble members and are averaged together to get daily ensemble-mean forecasts. As an operational system, the GFS undergoes continued changes in both model physics and initialization system (GDAS), which can be tracked online (at http://www.nco.ncep.noaa.gov/pmb/changes/). The CFSv2 is the latest generation of the Climate Forecast System at NCEP, which became operational in March 2011 (Saha et al. 2013). The atmospheric component is the GFS version as of May 2007 with a horizontal resolution of T126 (about 100 km). The ocean component is the MOM4. The CFSv2 includes a comprehensive land model and sea ice model. It is initialized from the NCEP Climate Forecast System Reanalysis (CFSR, Saha et al. 2010). The 45-day forecasts are available four times (00Z, 06Z, 12Z, and 18Z) a day with four ensemble members at each time, forming an ensemble of 16 members for each day. The daily average of the 16 members has been used as ensemble mean in following analysis.

The UH model is an atmosphere–ocean coupled model (Fu et al. 2003) developed at International Pacific Research Center, University of Hawaii at Manoa. The atmospheric component is a general circulation model (ECHAM-4) with T106 resolution (about 125 km) that was originally developed at the Max Planck Institute for Meteorology, Germany (Roeckner et al. 1996). The Tiedtke-Nordeng mass flux scheme (Tiedtke 1989; Nordeng 1994) is used to represent the deep, shallow, and midlevel convections. The ocean component is an intermediate upper-ocean model developed at University of Hawaii. It is comprised of a mixed-layer and a thermocline layer with a horizontal resolution of 0.5 × 0.5-degree. The UH model carried out 45-day forecasts during DYNAMO/CINDY period each week initialized with final operational global analysis on 1 × 1-degree produced by NCEP, also known as FNL (at http://dss.ucar.edu/datasets/ds083.2), which is almost the same as GDAS analysis but generated 1 h later.

In order to assess the MJO forecasting skills in these three models during the DYNAMO period, the anomalies of observed and forecasted OLR, zonal winds at 850 and 200-hPa are first obtained by removing observed climatological annual cycle (mean plus first three harmonics). Interannual anomalies represented with most recent 120-day mean (Lin et al. 2008; Gottschalck et al. 2010) are also removed. NOAA satellite OLR and FNL winds have been taken as the observations in this study. Combined anomalies are projected onto Wheeler–Hendon's EOF1 and EOF2 to get the time series of RMM1 and RMM2 (Wheeler and Hendon 2004); then we calculate the bivariate anomaly correlation coefficient (ACC) and root-mean-square error (RMSE) of the forecasts as a function of forecast lead time during this period (Lin et al. 2008; Gottschalck et al. 2010).

3 MJO forecasting skills in three models

Figure 2 shows the overall MJO forecasting skills during extended DYNAMO period (September 01st, 2011 to March 31st, 2012) as measured with the bivariate ACCs and RMSEs for the three models. As a common practice, the forecast lead time when the ACC drops to 0.5 has been defined as MJO forecasting skill in days. The resultant useful skills for the GFS, CFSv2, and UH models are, respectively, 13, 22, and 28 days during the DYNAMO/CINDY period. A simple equal-weighted multi-model ensemble (MME) with the CFSv2 and UH models reaches a useful skill of 36 days: A significant extension of individual models' skills. The higher skill of the MME is attributed to different yet complementary characteristics of the individual models on the representation of intraseasonal variability (Krishnamurti et al. 1999; Fu et al. 2013). Since the above skills are obtained by sampling the forecasts initialized once a week, a nature question that needs to be addressed is: Do the above skill assessments largely depend on the sampling intervals? Taking advantage of the daily forecasts available from the GFS and CFSv2 models, we recalculated the skills with a denser 1-day sampling. The resultant skills are about a half day shorter for the GFS model and 3 days longer for the CFSv2 model (Fig. 2). This result indicates that the skill obtained by using weekly forecasts is a useful approximation of models' overall capability on MJO forecasting. The results from the RMSE (Fig. 2b) are consistent with that of the ACC.

If the skills are assessed during DYNAMO IOP (September 1st, 2011 to January 15th, 2012), all three models have systematically lower skills (Fig. 3) than that assessed during extended DYNAMO period. During the IOP, the MJO skills are about 10, 15, and 22 days, respectively, for the GFS, CFSv2, and UH models. In another study, Wang et al. (2013) found that the MJO skill of the CFSv2 is about 22 days in boreal winter for 1999–2010 hindcasts. This result suggests that the MJO skill assessed during the extended DYNAMO period is likely a more reasonable representation of models' long-term performances.

Because the atmospheric component of the CFSv2 is similar to the operational GFS, at the same time, the GFS

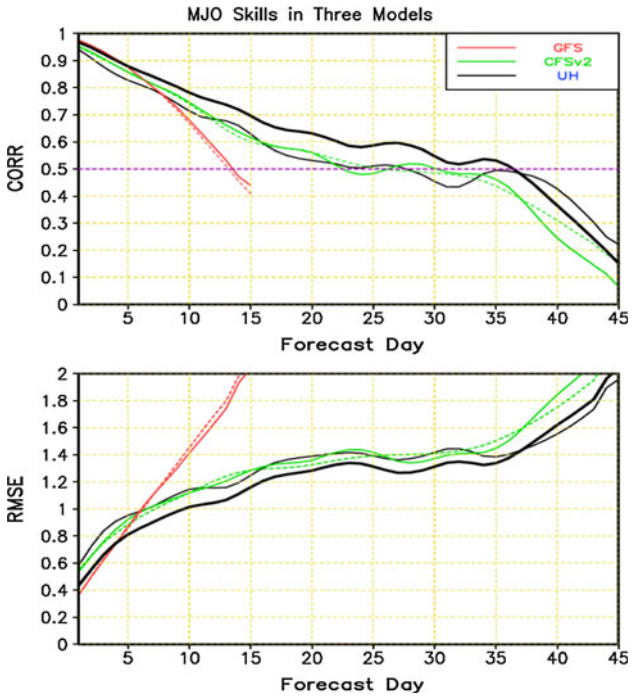

Fig. 2 MJO forecasting skills measured with Wheeler–Hendon index of the GFS, CFSv2 and UH models for DYNAMO/CINDY period (Sep 01, 2011–Mar 31, 2012). *Green* and *red solid* (*dashed*) *lines* are results with weekly (daily) sampling of CFSv2 and GFS models. The *thin black solid lines* are with weekly sampling of the UH model. The *thick black lines* are an equal-weighted ensemble of CFSv2 and UH models

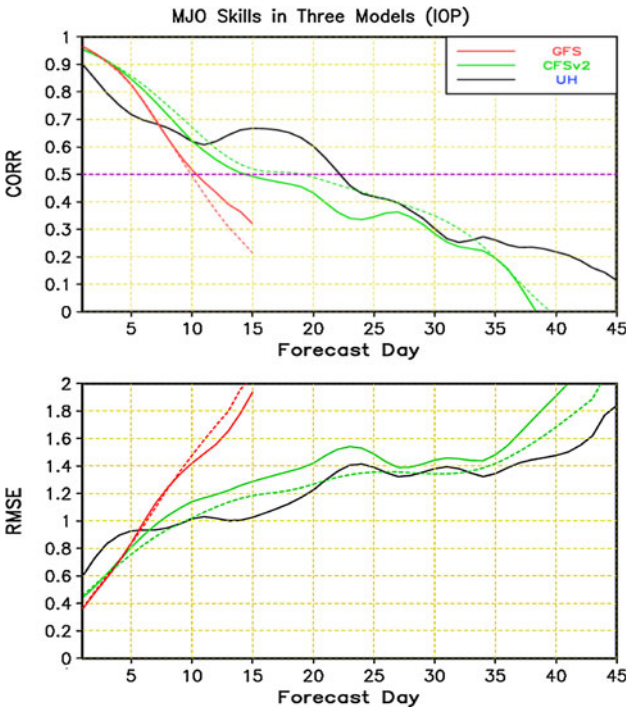

Fig. 3 MJO forecasting skills measured with Wheeler–Hendon index of the GFS, CFSv2 and UH models for DYNAMO/CINDY IOP period (Sep 01, 2011–Jan 15, 2012). *Green and red solid* (*dashed*) *lines* are results with weekly (daily) sampling of CFSv2 and GFS models. The *thin black solid lines* are with weekly sampling of the UH model

and CFSv2 forecasts used initial conditions from similar initialization systems (GDAS and CFSR), the skill differences between them may be largely attributed to the impact of air–sea coupling. Initially, these two forecasts have almost the same skill (with a high correlation of 0.96) with the skill of the GFS slightly higher in first week. The ACC of the GFS forecasts, however, falls much more rapidly than that of the CFSv2 with increased forecast lead time (Fig. 2). The present result suggests that air–sea coupling extends MJO forecasting skill by about 1 week. This finding is basically consistent with the result from our previous predictability study of Fu et al. (2007), which showed that air–sea coupling extends monsoon intraseasonal predictability by 1 week.

On the other hand, since both the CFSv2 and UH models include two-way air–sea interactions, the differences between them are largely attributed to different model physics. In first week, both the CFSv2 and GFS have higher skills than the UH model during the IOP (Fig. 3), but the UH model is consistently better beyond 10 days. This behavior of the UH model suggests that the initial conditions generated by a foreign model do cause some initial shocks, resulting in lower skills than those models (here, GFS and CFSv2) with initial conditions generated by more consistent initialization systems (GDAS and CFSR). The better skill of the UH model after first 10 days during the IOP, therefore, should be attributed to more realistic representation of intrinsic MJO mode in the model. This result is consistent with previous findings that ECHAM-4 family coupled models have an intrinsic MJO well mimic the observed one (Kemball-Cook et al. 2002; Fu and Wang 2004; and Kim et al. 2009).

The capability of the CFSv2 and UH models on forecasting the initiation and propagation of the MJO is examined with two specific forecasts that focus on November MJO. The first case is the forecasts initialized on November 4th, 2011 (Fig. 4). Initially, the dry and wet phases of the MJO-I were, respectively, located in the Indian Ocean and eastern Maritime Continent. Both the CFSv2 and UH models to some extent capture the eastward propagations of the dry phases of the MJO-I and the initiation of November MJO in the equatorial western Indian Ocean after 2 weeks, even the subsequent eastward propagations of November MJO wet phase. The forecasted eastward propagations (for both the MJO-I dry phase and November MJO wet phase) in the CFSv2 are slightly slower than that in the observations (Fig. 4a, b). On the other hand, the forecasts of the UH model are slightly faster than the observed (Fig. 4c, d). It is also interesting to note that the UH model is even able to reproduce another

eastward-propagating dry phase initiated over the western Indian Ocean in the late November and early December, 2011 (Fig. 4c).

The second case is the forecasts initialized on November 18th, 2011 (Fig. 5). At initial time, the wet phase of the observed November MJO was developing just west of the DYNAMO/CINDY array while the dry phase of the MJO-I still prevailed over the Maritime Continent and western Pacific. As the dry phase of MJO-I moves away, the convection of November MJO gradually propagates eastward, crosses the Maritime Continent, and reaches western Pacific in early December. Both the CFSv2 and UH models reproduce the observed intensifications of November MJO convection near the DYNAMO/CINDY array in the late November (Fig. 5b, d), likely associated with the development of Thanksgiving-TC. The convection forecasted by the CFSv2 hangs around the array site and does not propagate over the Maritime Continent (Fig. 5a, b). On the other hand, the UH model well captures the observed eastward propagation, even the subsequent development over the western Pacific (Fig. 5c, d).

4 Important role of air–sea coupling

Many previous studies with a hierarchy of models have shown that air–sea coupling improves the simulation and predictability of the MJO (Krishnamurti et al. 1988; Flatau et al. 1997; Wang and Xie 1998; Waliser et al. 1999; Woolnough et al. 2000; Fu and Wang 2004; Fu et al. 2007, 2008; Pegion and Kirtman 2008). Using model intraseasonal events as target, Fu et al. (2008) showed that the potential predictability of the atmosphere-only runs driven by forecasted daily SST reach very similar level as that of the coupled runs. To what extent the above result holds for the forecasts of real-world MJO is unknown. The different skills between the GFS and CFSv2 (Figs. 2, 3) also support the importance of air–sea coupling on MJO prediction. Since the GFS version used by the CFSv2 is not exact the GFS version used to produce forecasts for DYNAMO/CINDY period, it is inconclusive to attribute the improved skill in the CFSv2 over the GFS to the air–sea coupling alone. To assess how the treatment of ocean surface condition affects MJO forecast, a series of forecasting experiments to examine the roles of air–sea coupling as well as persistent, forecasted and observed daily SST on MJO prediction is carried out with UH model. Detailed experimental design is given in Table 1.

Figure 6 shows the bivariate ACCs and RMSEs during the entire DYNAMO period (September 01st, 2011 to March 31st, 2012) under four different SST settings (the skill of UH coupled forecasts has been repeated here from Fig. 2). When forced with persistent SST, the UH atmosphere-only forecasts have a skill of 20 days, which is apparently better than the skill of the GFS (Fig. 2). When forced with daily SST from the coupled forecasts, the UH atmosphere-only forecasts reach a skill almost the same as that of the coupled runs. This result directly corroborates our previous hypothesis: In the context of hindcasts and real-time forecasts, the atmosphere-only runs driven by daily SST forecasted from the

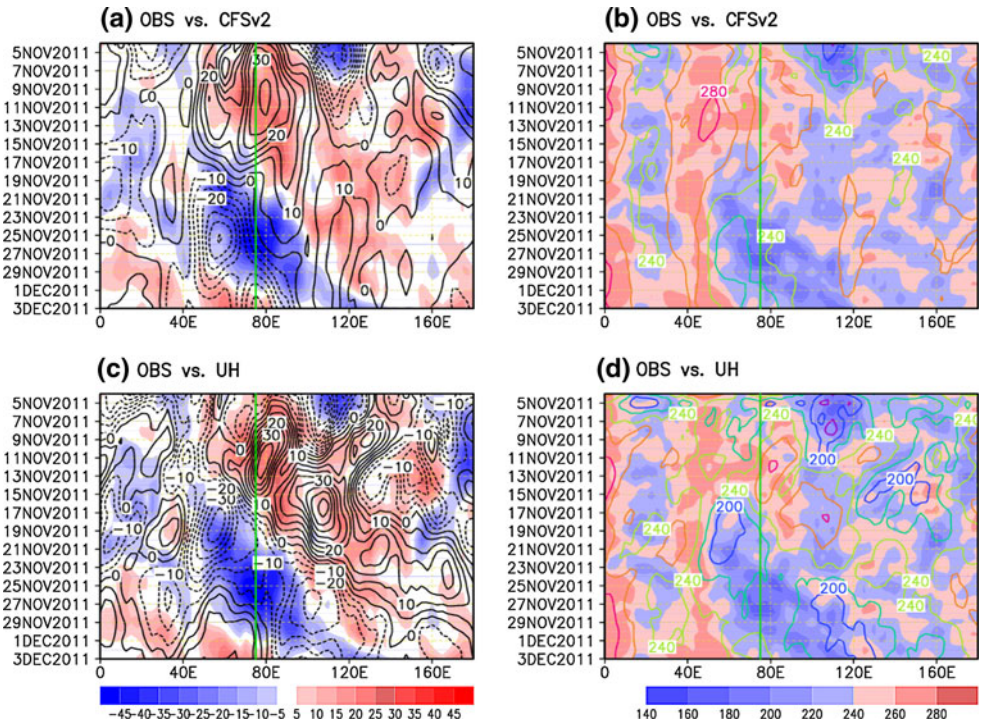

Fig. 4 Hovemoller diagrams of observed OLR (*shading*, unit: W m^{-2}) from November 4th to December 3rd, 2011 and corresponding forecasts (*contours*, CI 10 W m^{-2}) by the CFSv2 and UH models averaged between 10°S and 10°N. *Left panels* show anomalies and *right panels* display total fields of OLR

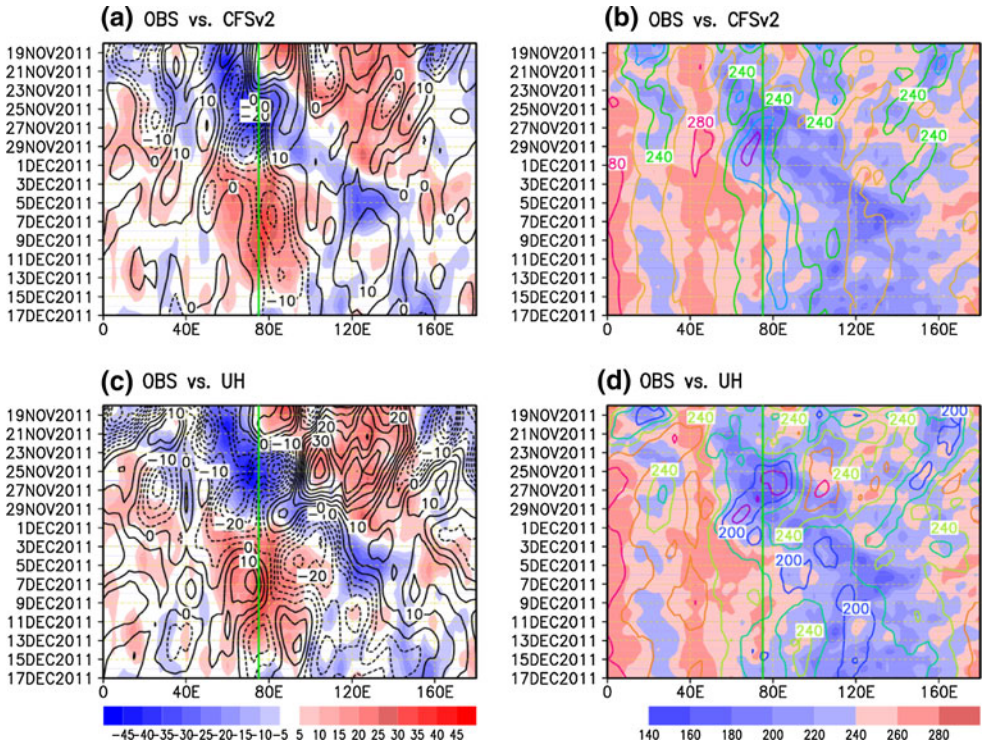

Fig. 5 Hovemoller diagrams of observed OLR (*shading*, unit: W m^{-2}) from November 18th to December 17th, 2011 and corresponding forecasts (*contours*, CI 10 W m^{-2}) by the CFSv2 and UH models averaged between 10°S and 10°N. *Left panels* show anomalies and *right panels* display total fields of OLR

Table 1 Forecasting experiments with UH model under different SST settings

Names of experiments	SST settings
CPL	Atmosphere–ocean coupled forecasts
Fcst_SST (or fsst)	Atmosphere-only forecasts driven by daily SST derived from the 'cpl' forecasts
Pers_SST (or psst)	Atmosphere-only forecasts driven by persistent SST
TMI_SST (or osst)	Atmosphere-only forecasts driven by observed daily TMI SST

coupled runs reach a similar skill as that of the coupled runs. The present finding suggests that *if forcing the high-resolution GFS with CFSv2 forecasted daily SST, the MJO forecasting skill of the GFS can be improved significantly.* It is also very encouraging to note that when forced with observed daily SST from TRMM Microwave Imager (TMI, Gentemann et al. 2004), MJO forecasting skill reaches beyond 40 days during the DYNAMO period. This result not only suggests that there are plenty rooms to improve ocean component of UH model, but also the atmospheric component and air–sea coupling processes, because SST is a result of two-way atmosphere–ocean interactions (Fu et al. 2003; Zheng et al. 2004).

To examine the impact of air–sea coupling on the initiation and propagation of the MJO, we take the forecasts initialized on November 4th, 2011 as an example. Figure 7 shows the phase-diagrams of the observations and four forecasts with different SST settings for a period of 1 month. Initially, all four forecasts have weaker MJO amplitude than that of the observations. Because observed OLR is not included in the initialization of UH model, the resultant initial OLR anomaly in this case is smaller than the observed (not shown). During the first week, all four runs have very similar trajectory. After that, the MJO signal in the atmosphere-only run forced by persistent SST decays very quickly. Other three runs follow each other very well and all have similar propagation speed as the observations. In the end of one-month forecasts, all three forecasts reach the Maritime Continent as in the observations (near the transition zone from phase 4 to phase 5), but the forecasts have problem to maintain the observed amplitudes when approaching the Maritime Continent. The distinctive differences between the persistent-SST runs and other runs with intraseasonally-varying SST demonstrate that air–sea coupling or intraseasonal SST forcing plays an important role in the forecasting of MJO initiation and propagation in UH model.

Figure 8 further examines the evolutions of total SST and anomalous OLR over tropical Indian Ocean (75°E–

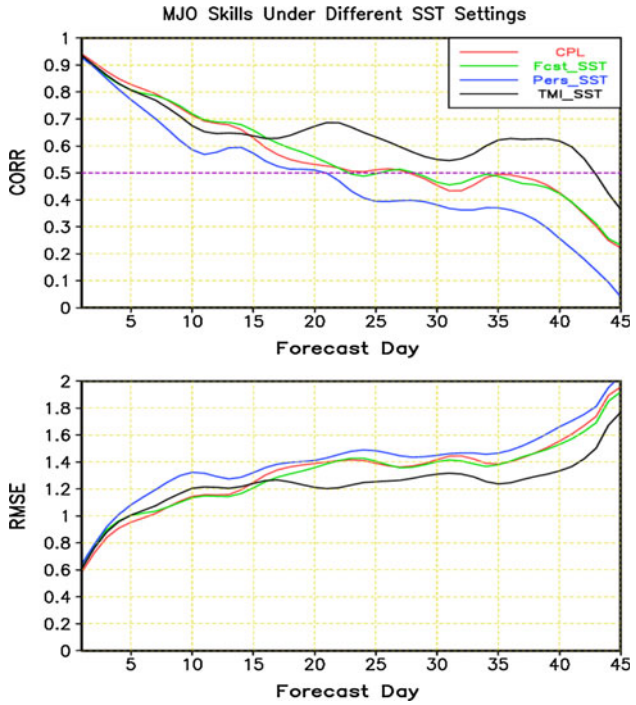

Fig. 6 MJO forecasting skills of the UH model measured with Wheeler–Hendon index for DYNAMO/CINDY period (Sep 01, 2011–Mar 31, 2012) under different SST settings (Table 1)

95°E, 5°S–5°N) during 1 month forecasts under different SST settings initialized on November 4th, 2011. The observed TMI SST shows a warm anomaly of about 1 °C (Fig. 8a) associated with positive OLR anomaly (Fig. 8b) during first 15 days; followed by a cooling period in association with the initiation and development of November MJO convective envelope. The ensemble-mean SST in the coupled forecasts shows a similar evolution with the observations but with much smaller amplitude. Future

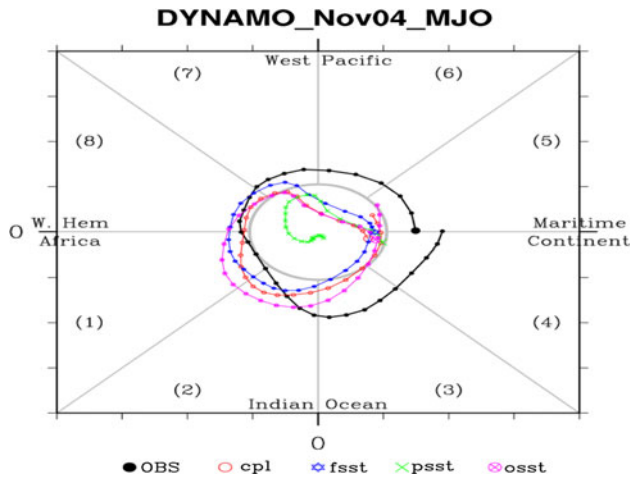

Fig. 7 Phase diagrams of observed and forecasted Wheeler–Hendon index from November 4th to December 3rd, 2011. The forecasts are carried out with UH model under different SST settings (Table 1)

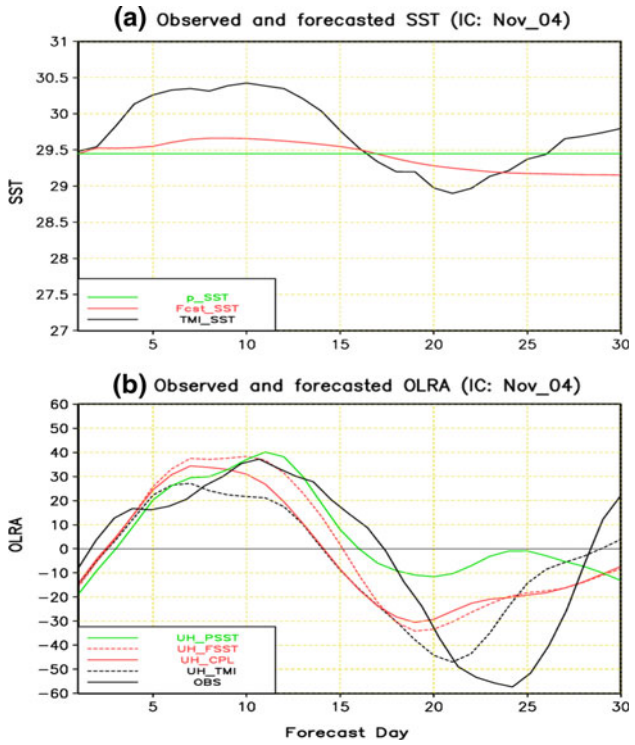

Fig. 8 Observed and forecasted sea surface temperature (unit: °C) in total (**a**); and OLR anomalies (unit: W m^{-2}) over tropical Indian Ocean (75°E–95°E, 5°S–5°N) from November 4th to December 3rd, 2011. Forecasts are carried out by UH model under different SST settings (Table 1)

research is needed to identify the misrepresented air–sea coupling processes through validating model oceanic mixed-layer heat budget with DYNAMO in situ observations. The forecasts of the coupled runs and atmosphere-only runs driven by forecasted daily SST produce an early initiation of November MJO with considerably underestimated convection (Fig. 8b). When driven with TMI daily SST, the amplitude of the forecasted MJO convective envelope shows a significant improvement but still with an early initiation. Consistent with the result revealed from previous phase diagram (Fig. 7), the atmosphere-only forecasts driven with persistent SST barely capture the initiation of November MJO in the Indian Ocean.

5 November-MJO and Thanksgiving-TC

During the IOP of the DYNAMO field campaign, one very interesting MJO–TC interaction case is observed in association with November MJO: the near-equatorial tropical cyclogenesis (named as "TC05A" by JTWC,[5] also known as Thanksgiving-TC in DYNAMO community) around

[5] JTWC stands for Joint Typhoon Warning Center; more details of "TC05A" can be found online: http://en.wikipedia.org/wiki/2011_North_Indian_Ocean_cyclone_season#cite_note-47.

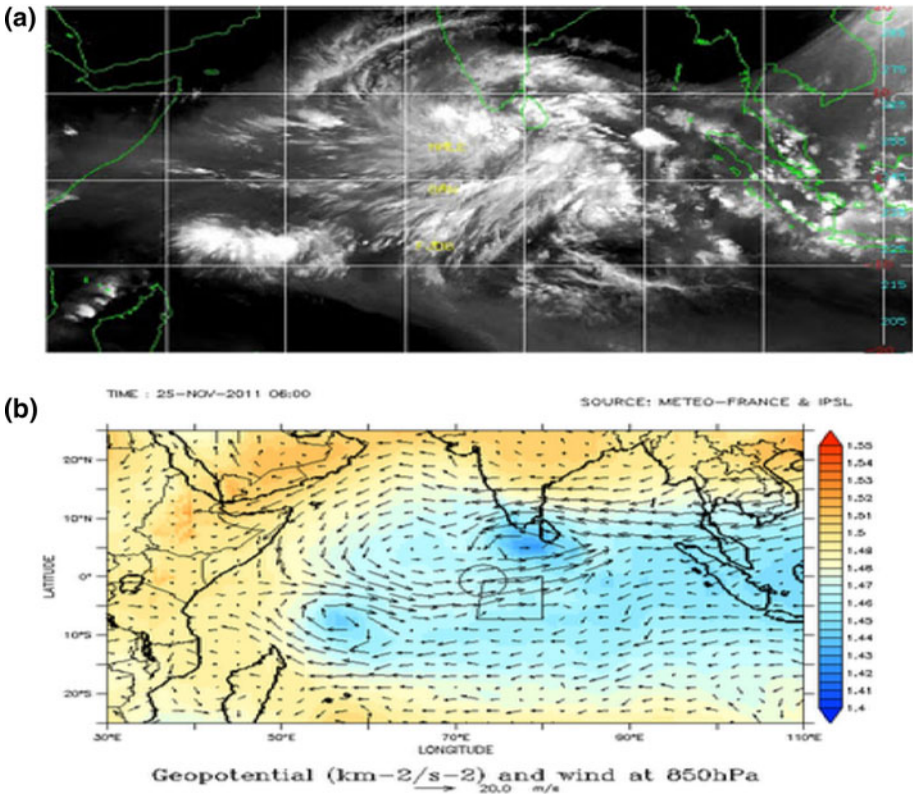

Fig. 9 (*upper panel*) Infrared satellite image, and (*lower panel*) analyzed 850-hPa wind vectors and Geopotential on November 25, 2011. The *box* in the *lower panel* represents the DYNAMO array (Courtesy of MJO-Conversation at http://maddenjulianconversation blogspot.com/2011/11/cyclone-and-westerly-wind-burst.html)

November 26. Because this event was well observed by the DYNAMO array and airborne instruments, several observational studies have focused on this event.[6] Figure 9 shows the satellite image and 850-hPa winds on November 25, 2011, which is about 1 day before the genesis of TC05A. The active convection of November MJO develops in the tropical Indian Ocean (Fig. 9a). The MJO-associated westerly wind bursts directly blow over the DYNAMO array (Fig. 9b). A pair of vortices develops in association with the westerly wind bursts (Ferreira et al. 1996; Shen et al. 2012). The vortex near Sri Lanka is significantly enhanced by the shear flows between the near-equatorial westerly and strong easterly around 10°N, which further intensifies into a tropical cyclone-TC05A near the southern tip of the Indian peninsula and move northwestward into the Arabian Sea. In this section, we examine to what extent the interaction between November-MJO and Thanksgiving-TC can be captured in the extended-range forecasts of the GFS, CFSv2, and UH models.

Figure 10 shows the observed and forecasted MJO evolutions initialized 2 weeks before the genesis of Thanksgiving-TC in terms of Wheeler–Hendon phase diagrams. Initially, the observed MJO resides in the western Pacific (phase 7) and quickly moves into Indian Ocean sector (phase 2) after 10 days. The forecasted MJO enters the Indian Ocean after 11 and 14 days, respectively, in the UH and CFSv2 models. The MJO in the GFS tends to intensify in African sector and doesn't propagate into Indian Ocean during 2 weeks' forecasts. One more thing worth noting is that both the UH and CFSv2 models fail to predict MJO propagation over the Maritime Continent. This MJO forecasting barrier seems epidemic for all models. A better understanding and representation of the interactions between the MJO and Maritime Continent (including the islands and marginal seas) holds the key to break this barrier (e.g., Zhu et al. 2010). Since this problem represents a huge stumbling block for the further advancement of MJO forecast, a community-wide approach (like the combined IOP and modeling efforts of the DYNAMO/CINDY program) is definitely needed.

Figure 11 gives the observed and forecasted three-day means of 850-hPa zonal winds and deep convection (OLR $\leq$ 240 W m^{-2}) in the end of second week initialized on November 11th, 2011. In the observations, MJO-associated convection and westerly winds have well developed in tropical Indian Ocean (Figs. 11a, 9) while the GFS forecasts (Fig. 11b) don't produce any MJO signal there with 2 weeks' lead. Both the CFSv2 and UH models to some extent reproduce the MJO-associated westerly wind bursts and deep convection (Fig. 11c, d). Although the ensemble-mean westerly in the UH model and convection

[6] For example, the study of Jim Moum at: http://www.eol.ucar.edu/projects/dynamo/meetings/2012/jul/index.html).

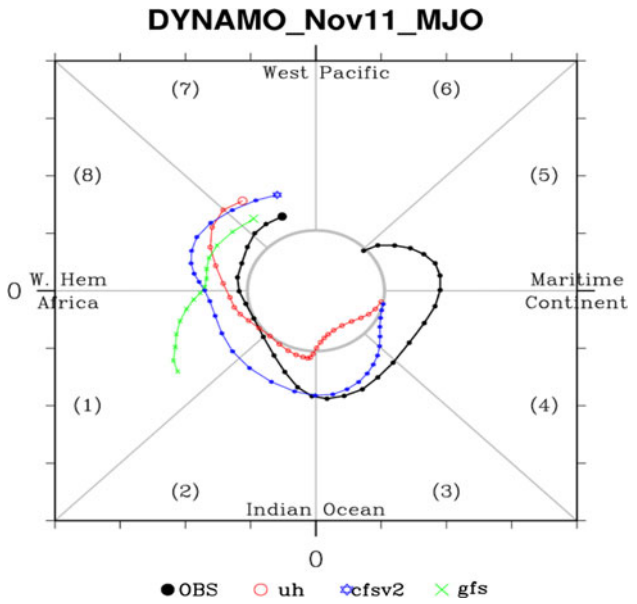

Fig. 10 Phase diagrams of observed and forecasted Wheeler–Hendon index from November 11th to December 10th, 2011. The forecasts are carried out by the GFS, CFSv2, and UH models

in the CFSv2 have been underestimated, a detailed examination reveals that both models produce a pair of vortices similar as the observed, which further develop into model tropical cyclones as defined in Fu and Hsu (2011). The distinctive difference between the GFS and CFSv2 suggests that the lack of air–sea coupling in the GFS fails it to predict the initiation of November MJO in Indian Ocean and the associated genesis of Thanksgiving-TC with 2 weeks' lead.

When initialized on November 18th—about 1 week before the genesis of the TC05A, all three models capture the initiation of November MJO in the Indian Ocean after a few days' integrations (Fig. 12). The MJO signal in the GFS forecasts, however, decays too quickly. The forecasts of the UH and CFSv2 also fail to maintain the observed amplitude when approaching the Maritime Continent. Figure 13 shows the three-day mean observed and forecasted spatial distributions of 850-hPa zonal winds and convection in the end of 2 weeks' forecasts. A detailed examination reveals that all three models capture the development of November-MJO and Thanksgiving-TC (not shown). When the TC moves away to northern Arabian Sea and dissipates there in the end of November, the observed MJO remains strong and continues propagating eastward (Fig. 13a). In the GFS forecasts, however, the MJO disappears after the development of Thanksgiving-TC. This behavior of the GFS suggests that the TC draws all energy from the MJO and results in the rapid decaying of the MJO. This also implies that the lack of large-scale air–sea coupling makes the model MJO vulnerable to the subsidence and dry air intrusion induced by Thanksgiving-TC. Further in-depth diagnosis and numerical experiments are needed to sort this out, which is beyond the scope of present study. On the other hand, both the CFSv2 and UH models include air–sea coupling and are able to maintain the convective envelope and large-scale circulations of November-MJO after the development of Thanksgiving-TC (Fig. 13c, d).

When initialized on November 25th, 2011, the phase evolution of November MJO is best forecasted by the CFSv2 (Fig. 14). The GFS forecasts are also able to maintain a strong MJO in phase 2 and 3, but with very slow eastward propagation. The forecasts of the UH model in this case have difficulty to maintain significant MJO signal in the model (Fig. 14). The three-day mean 850-hPa zonal winds and convection in the end of 2 weeks' forecasts along with the observations are given in Fig. 15. The observed MJO convective envelope has moved out of the Indian Ocean and entered Maritime Continent and western Pacific (Fig. 15a) along with strong westerly winds in southern Indian Ocean. This feature has been well reproduced in the CFSv2 forecasts (Fig. 15c) and to some extent also in the GFS forecasts (Fig. 15b). The latter, however, fail to reproduce a secondary westerly-wind patch over the Maritime Continent. In contrast to the observations, the UH model still produces very strong convection in Indian Ocean (Fig. 15d), particularly in western side of the basin.

The possible causes for this bias in UH model are two folds. First, a detailed examination of each ensemble indicates that the model tends to produce too much tropical cyclone-like disturbances in southwest Indian Ocean. This bias is also present in boreal summer, which leads to an early false onset of northward-propagating boreal-summer monsoon intraseasonal events (Fu et al. 2013). Second, the bias may be related to the not-so-strong divergence and dry air intrusion associated with Rossby-wave-like response to the MJO convection, which is supposed to induce large boundary-layer divergence and bring subtropical dry air into the backside of the MJO convection and to shut off deep convection there, thus helping move the MJO eastward (Matthews 2000). Further research to unravel the detailed causes of this model bias is warranted, which will be one of our future research topics.

6 Discussions and concluding remarks

6.1 Discussions

The observed SST-precipitation quadrature phase relationship on intraseasonal timescales (Shinoda et al. 1998; Senguta et al. 2001) has suggested that interactive air–sea coupling represents an important process for MJO dynamics (Wang and Xie 1998). On the one hand, the

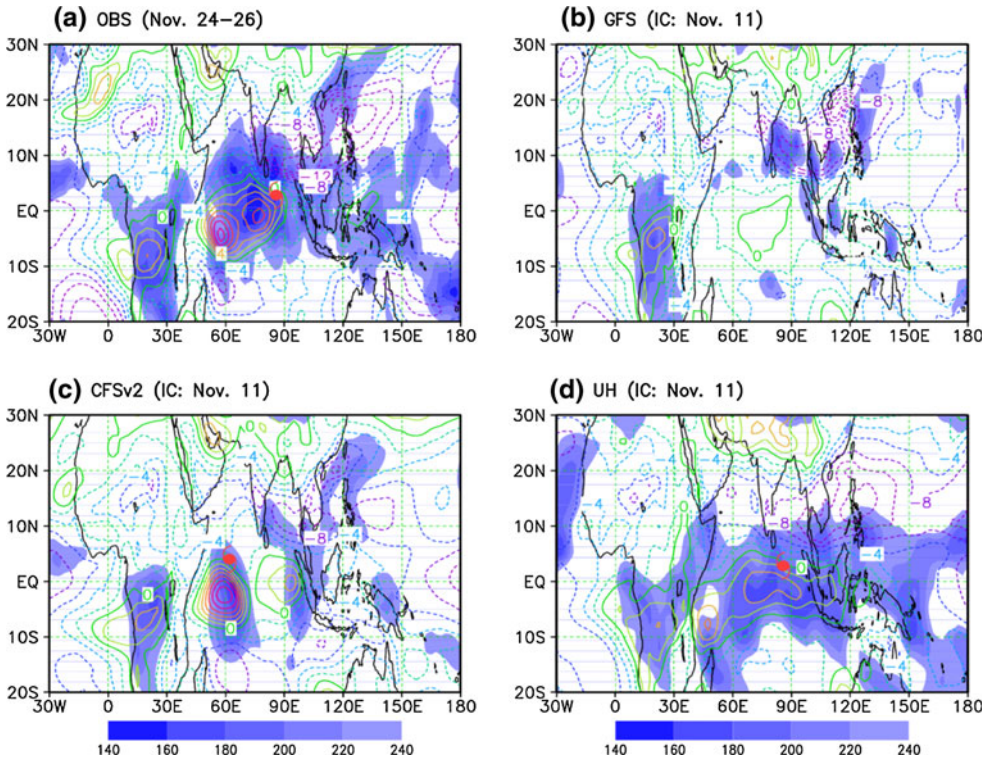

Fig. 11 Observed (**a**) and forecasted OLR (*shading*, unit: W m^{-2}) and 850-hPa zonal winds (contours, CI: 2 m s^{-1}) averaged during November 24th and 26th, 2011. The forecasts are carried out by the GFS (**b**), CFSv2 (**c**) and UH (**d**) models initialized on November 11th, 2011

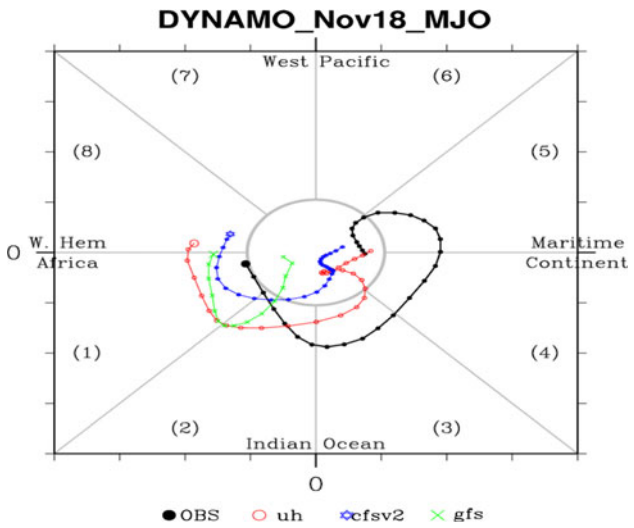

Fig. 12 Phase diagrams of observed and forecasted Wheeler–Hendon index from November 18th to December 17th, 2011. The forecasts are carried out by the GFS, CFSv2, and UH models

atmospheric forcing of the MJO changes underlying SST through modifying surface heat fluxes (Senguta et al. 2001; Waliser et al. 2003), oceanic mixed-layer entrainment (Fu et al. 2003; Saji et al. 2006), and horizontal advection (Han et al. 2007). On the other hand, the resultant intraseasonal SST anomaly feeds back to organize MJO convection and associated circulations through enhancing boundary-layer convergence (Wang and Xie 1998; Waliser et al. 1999) and surface evaporation (Fu et al. 2008). Interactive air–sea coupling is also found to be a necessity to maintain the observed SST-precipitation quadrature phase relationship while the forced atmosphere-only simulations produce an in-phase intraseasonal SST-precipitation relationship (Wu et al. 2002; Fu et al. 2003; Zheng et al. 2004; Matthews 2004). This result might be interpreted as that atmosphere-only approach is not an appropriate way to carry out MJO forecasting.

Our forecasting experiments, however, demonstrate that this is not the case for the well initialized runs. In fact, the atmosphere-only forecasts driven by daily SST derived from the coupled forecasts reach a similar skill level as the coupled forecasts (Fig. 6). Like the coupled forecasts, the initialized atmosphere-only runs are also able to maintain the observed SST-precipitation quadrature phase relationship to some extent (e.g., Fig. 8). *It is the match between MJO-related large-scale circulations in the initial conditions and specified underlying SST sustains the observed quadrature SST-precipitation relationship in the atmosphere-only forecasts* (e.g., Figs. 15 and 16 in Fu et al. 2008). The atmosphere-only free simulations forced with daily SST, however, are not an appropriate way to assess the impacts of intraseasonal SST forcing due to the mix-up of atmosphere internal MJO mode and SST-forced intraseasonal response.

The above findings raise the possibility to first improve the forecasts of intraseasonal SST anomalies through improving individual coupled models or developing multi-model ensemble; then using the resultant intraseasonal SST

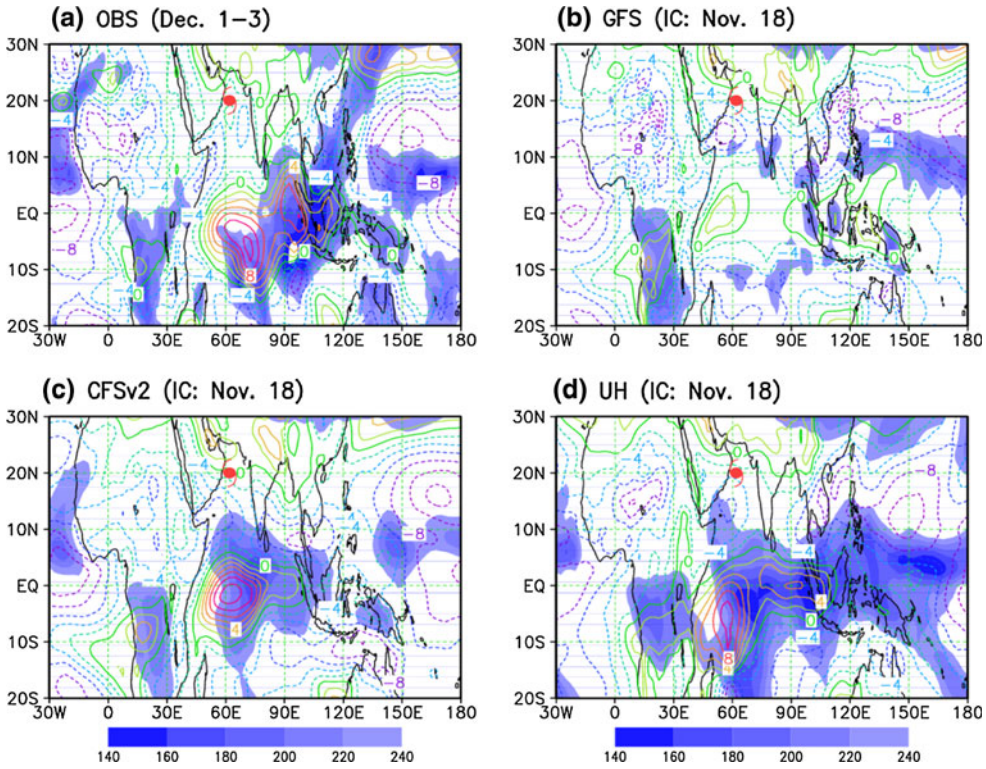

Fig. 13 Observed (**a**) and forecasted OLR (*shading*, unit: W m^{-2}) and 850-hPa zonal winds (contours, CI: 2 m s^{-1}) averaged during December 1st and 3rd, 2011. The forecasts are carried out by the GFS (**b**), CFSv2 (**c**) and UH (**d**) models initialized on November 18th, 2011

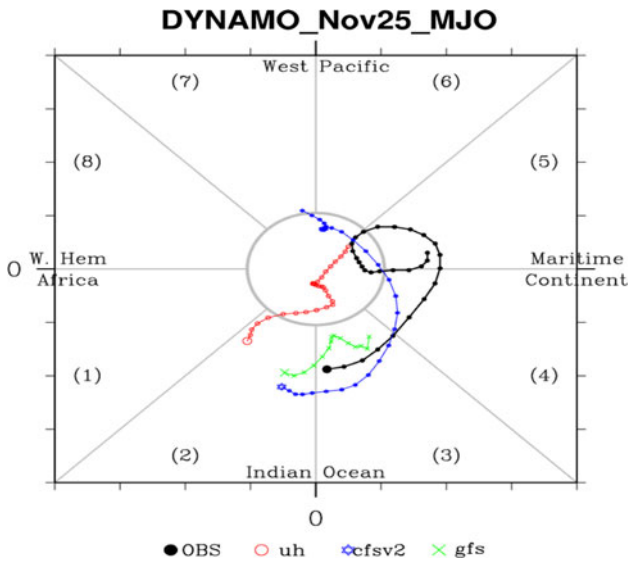

Fig. 14 Phase diagrams of observed and forecasted Wheeler–Hendon index from November 25th to December 24th, 2011. The forecasts are carried out by the GFS, CFSv2, and UH models

anomalies as boundary conditions to force atmosphere-only forecasts. Along this line, we expect that *the high-resolution GFS driven by daily SST forecasted from the lower-resolution CFSv2 can reach a much higher MJO forecasting skill than its current level as forced by persistent SST*. This could be true for all two-week extended-range forecasting systems participating in the THORPEX TIGGE program. Further if the improved MJO forecasting in these systems also results in better extended-range TC forecast, using forecasted daily SST as sea surface conditions will be an approach worth being implemented for all TIGGE forecasting models.

6.2 Concluding remarks

During the DYNAMO/CINDY field campaign, five MJO events have been observed (Fig. 1). The associated convective envelope resides over Indian Ocean, respectively, in the late October (MJO-I), late November (MJO-II), late December (MJO-III), late January (MJO-IV), and late February-early March (MJO-V). The convective envelopes of the two events in December and January have limited longitudinal extent. Whether they should be categorized as MJO is still an open issue that, however, won't affect our conclusions. Current models have relatively higher skill in forecasting the MJO that follows a preceding event (successive MJO) than that without preceding event (primary MJO). The common model problems include too slow eastward propagation, the Maritime Continent barrier, the difficulty to predict the MJO initiated by Rossby (or mixed-Rossby-gravity) waves, and the underestimation of the observed intensity.

The MJO forecasting skills of the GFS, CFSv2 and UH models during the DYNAMO/CINDY period have been assessed with the Wheeler–Hendon bivariate ACCs and RMSEs (Lin et al. 2008). The overall MJO skills for the

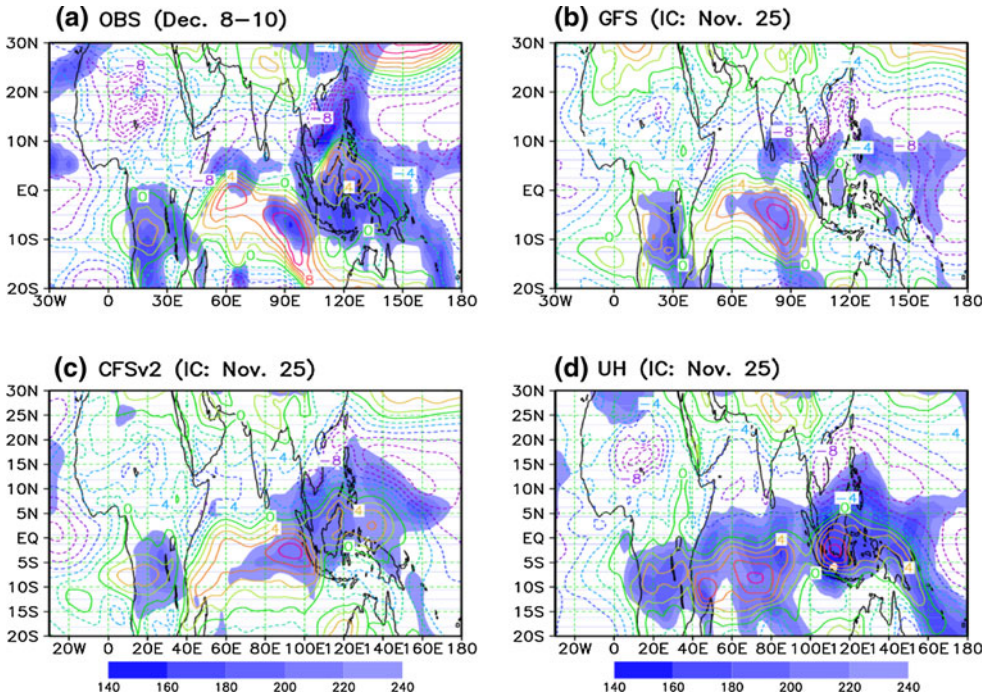

Fig. 15 Observed (**a**) and forecasted OLR (*shading*, unit: W m^{-2}) and 850-hPa zonal winds (contours, CI: 2 m s^{-1}) averaged during December 8th and 10th, 2011. The forecasts are carried out by the GFS (**b**), CFSv2 (**c**) and UH (**d**) models initialized on November 25th, 2011

three models are, respectively, 13, 25, and 28 days (Fig. 2) when the ACC dropping to 0.5 has been used as the criterion. Two case studies have been given to show that the initiation of November MJO can be predicted with a lead time of 2 weeks by both the CFSv2 and UH models (Fig. 4). The relatively lower skill of the CFSv2 than the UH model may be largely attributed to the slow MJO eastward propagation in the CFSv2 forecasts (Fig. 5).

The superior performance of the CFSv2 over the GFS (Fig. 2) suggests that air–sea coupling significantly extends MJO forecasting skill. In order to quantify the impacts of air–sea coupling, three more sensitive forecasting experiments in addition to the coupled forecasts (Table 1) have been carried out with the UH model: atmosphere-only runs forced by persistent SST, forecasted and observed daily SST. Because initial conditions of these runs are the same, the skill differences among them directly measure the impacts of air–sea coupling and different SST settings. It turns out that the case driven by persistent SST has the lowest skill of 20 days (Fig. 6); the case driven by forecasted daily SST has a similar skill as the coupled forecasts (28 days); the case driven by observed daily TMI SST reaches beyond 40 days.

The UH and CFSv2 coupled models are also superior over the high-resolution GFS atmosphere-only model in representing the interactions of November MJO-Thanksgiving TC on extended-range timescales. The CFSv2 and UH coupled models are able to capture the development of westerly wind bursts associated with November-MJO and the genesis of Thanksgiving-TC with 2 weeks' lead while the GFS totally fails (Figs. 10, 11), although apparent biases still exist in the forecasted MJO by the CFSv2 and UH models (e.g., intensity and spatial pattern) and the location of the TC (Fig. 11). Both the CFSv2 and UH coupled models are also able to maintain November MJO as in the observations after Thanksgiving-TC moving away, while the MJO in the GFS disappears (Figs. 12, 13).

In order to further advance our understanding of the physical processes governing the initiation and propagation of the MJO and to improve their representations in state-of-the-art global models, more in-depth diagnostics and numerical experiments are needed to address following questions: (1) How does air–sea coupling extend the MJO forecasting skills? (2) What are the major air–sea coupling processes misrepresented in the CFSv2 and UH coupled models? (3) Why does the MJO in the CFSv2 propagate so slow? (4) Why is the UH model prone to false TC genesis in southwest Indian Ocean? (5) What are the different physical processes leading to the initiations of the primary and successive MJO events? Some of these questions are under investigation and findings will be reported elsewhere.

Acknowledgments This work was sponsored by NOAA (NA11OAR4310096 & NA10OAR4310247), NSF (AGS-1005599) and by the Japan Agency for Marine-Earth Science and Technology (JAMSTEC), NASA, and NOAA through their supports of the IPRC. Additional supports are from APEC Climate Center and CMA project (GYHY201206016). We thank Dr. Matt Wheeler for sharing his codes to filter out MJO and equatorial waves in Fig. 1. This paper is SOEST contribution number 8961 and IPRC contribution number 992.

References

Belanger JI, Webster PJ, Curry JA (2012) Extended predictions of North Indian Ocean tropical cyclones. Weather Forecast 27: 757–769

Brunet G, Hoskins M, Moncrieff M, Dole R, Kiladis GN, Kirtman B, Lorenc A, Mills B, Morss R, Polavarapu S, Rogers D (2010) Collaboration of the weather and climate communities to advance subseasonal to seasonal prediction. Bull Am Meteorol Soc 91:1397–1406

Donald A, Meinke H, Power B, de Maia AHN, Wheeler MC, White N, Stone RC, Ribbe J (2006) Near-global impact of the Madden-Julian oscillation on rainfall. Geophys Res Lett 33:L09704. doi:10.1029/2005GL025155

Ferreira RN, Schubert WH, Hack JJ (1996) Dynamical aspects of twin tropical cyclones associated with the Madden-Julian oscillation. J Atmos Sci 53:929–945

Flatau M, Flatau PJ, Phoebus P, Niiler PP (1997) The feedback between equatorial convection and local radiative and evaporative processes: the implication for intraseasonal oscillations. J Atmos Sci 54:2373–2386

Fu X (2012) Extended-range TC forecasting: opportunity and challenge. US CLIVAR summit, Newport Beach, CA, July 17–20, 2012. Available online at: http://www.usclivar.org/sites/default/files/meetings/Fu_ExRangeTCF_2012Summit_pres.pdf

Fu X, Hsu P (2011) Extended-range ensemble forecasting of tropical cyclogenesis in the northern Indian Ocean: modulation of Madden-Julian oscillation. Geophys Res Lett 38:L15803. doi:10.1029/2011GL048249

Fu X, Wang B (2004) Differences of boreal-summer intraseasonal oscillations simulated in an atmosphere-ocean coupled model and an atmosphere-only model. J Clim 17:1263–1271

Fu X, Wang B, Li T, McCreary JP (2003) Coupling between northward-propagating intraseasonal oscillations and sea surface temperature in the Indian Ocean. J Atmos Sci 60:1733–1753

Fu X, Wang B, Waliser DE, Tao L (2007) Impact of atmosphere–ocean interaction on the predictability of monsoon intraseasonal oscillation. J Atmos Sci 64:157–174

Fu X, Yang B, Bao Q, Wang B (2008) Sea surface temperature feedback extends the predictability of tropical intraseasonal oscillation. Mon Weather Rev 136:577–597

Fu X, Wang B, Lee J-Y, Wang WQ, Gao L (2011) Sensitivity of dynamical intraseasonal prediction skills to different initial conditions. Mon Weather Rev 139:2572–2592

Fu X, Wang WQ, Lee J-Y, Wang B, Vitart F (2013) Intraseasonal forecasting of Asian summer monsoon in four operational and research models. J Clim 26:4186–4203

Gentemann CL, Wentz FJ, Mears CM, Smith DK (2004) In-situ validation of tropical rainfall measuring mission microwave sea surface temperatures. J Geophys Res 109:C04021. doi:10.1029/2003JC002092

Gottschalck J, Wheeler M, Weickmann K, Vitart F, Savage N, Lin H, Hendon H, Waliser D, Sperber K, Nakagawa M, Prestrelo C, Flatau M, Higgins W (2010) A framework for assessing operational Madden-Julian oscillation forecasts: a CLIVAR MJO working group project. Bull Am Meteorol Soc 91: 1247–1258

Han WQ, Yuan DL, Liu WT, Hakides DJ (2007) Intraseasonal variability of Indian Ocean sea surface temperature during boreal winter: Madden-Julian oscillation versus submonthly forcing and processes. J Geophys Res 112:C04001. doi:10.1029/2006JC003791

Hendon HH, Salby ML (1994) The life cycle of the Madden-Julian oscillation. J Atmos Sci 51:2225–2237

Higgins RW, Shi W (2001) Inter-comparison of the principal modes of interannual and intraseasonal variability of the North American monsoon system. J Clim 14:403–417

Hoskins B (2012) The potential for skill across the range of the seamless weather-climate prediction problem: a stimulus for our science. Q J Roy Meteorol Soc. doi:10.1002/qj.1991

Kemball-Cook S, Wang B, Fu X (2002) Simulation of the intraseasonal oscillation in the ECHAM-4 model: the impact of coupling with an ocean model. J Atmos Sci 59:1433–1453

Kikuchi K, Wang B, Fudeyasu H (2009) Genesis of tropical cyclone Nargis revealed by multiple satellite observations. Geophys Res Lett 36:L06811. doi:10.1029/2009GL037296

Kim D et al (2009) Application of MJO simulation diagnostics to climate models. J Clim 22:6413–6436

Klotzbach PJ (2010) On the Madden-Julian oscillation-Atlantic hurricane relationship. J Clim. doi:10.1175/2009JCL2978.1

Krishnamurti TN, Oosterhof DK, Mehta AV (1988) Air–sea interaction on the time scale of 30 to 50 days. J Atmos Sci 45: 1304–1322

Krishnamurti TN, Kishtawal CM, LaRow T, Bachiochi D, Zhang Z, Williford CE, Gadgil S, Surendran S (1999) Improved skills for weather and seasonal climate forecasts from multimodel superensemble. Science 285:1548–1550

Kubota H, Yoneyama K, Jun-Ichi H (2012) Contribution of tropical cyclone for the preconditioning of the Madden-Julian oscillation during CINDY2011. Presentation on AGU fall meeting, San Francisco, December 03, 2012

Lau WKM, Waliser DE (eds) (2011) Intraseasonal variability of the atmosphere–ocean climate system, 2nd edn. Springer, Heidelberg, p 613

Liebmann B, Hendon HH, Glick JD (1994) The relationship between tropical cyclones of the western Pacific and Indian Oceans and the Madden-Julian oscillation. J Meteorol Soc Japan 72:401–412

Lin J-L et al (2006) Tropical intraseasonal variability in 14 IPCC AR4 climate models. Part I: convective signals. J Clim 19:2665–2690

Lin H, Brunet G, Derome J (2008) Forecast skill of the Madden-Julian oscillation in two Canadian atmospheric models. Mon Weather Rev 136:4130–4149

Madden RA, Julian PR (1971) Detection of a 40–50-day oscillation in the zonal wind in the tropical Pacific. J Atmos Sci 28:702–708

Madden RA, Julian PR (1972) Description of global-scale circulation cells in the tropics with a 40–50 day period. J Atmos Sci 29:1109–1123

Majda AJ, Biello JA (2004) A multiscale model for the intraseasonal oscillation. Proc Natl Acad Sci USA 101:4736–4741

Maloney ED, Hartmann DL (2000) Modulation of hurricane activity in the Gulf of Mexico by the Madden-Julian oscillation. Science 287:2002–2004

Matsueda M, Endo H (2011) Verification of medium-range MJO forecasts with TIGGE. Geophys Res Lett 38:L11801. doi:10.1029/2011GL047480

Matthews AJ (2000) Propagation mechanisms for the Madden-Julian oscillation. Q J Roy Meteorol Soc 126:2637–2652

Matthews AJ (2004) Atmospheric response to observed intraseasonal tropical sea surface temperature anomalies. Geophys Res Lett 31:L14107. doi:10.1029/2004GL020474

Matthews AJ (2008) Primary and successive events in the Madden-Julian oscillation. Q J Roy Meteorol Soc 134:439–453

Mo KC (2000) The association between intraseasonal oscillations and tropical storms in the Atlantic basin. Mon Weather Rev 128: 4097–4107

Molinari J, Knight D, Dickinson M, Vollaro D, Skubis S (1997) Potential vorticity, easterly waves, and eastern Pacific tropical cyclogenesis. Mon Weather Rev 125:2699–2708

Nakazawa T (2006) Madden-Julian oscillation activity and Typhoon landfall on Japan in 2004. SOLA 2:136–139. doi:10.2151/sola.2006-035

Nordeng TE (1994) Extended versions of the convective parameterization scheme at ECMWF and their impact on the mean and transient activity of the model in the tropics. Technical Memorandum No. 206, European Centre for Medium-Range Weather Forecasts, Reading, United Kingdom

Pegion K, Kirtman BP (2008) The impact of air–sea interactions on the simulation of tropical intraseasonal variability. J Clim 21: 6616–6635

Rashid HA, Hendon HH, Wheeler MC, Alves O (2010) Prediction of the Madden-Julian oscillation with the POAMA dynamical prediction system. Clim Dyn. doi:10.1007/s00382-010-0754-x

Roeckner E et al. (1996) The atmospheric general circulation model ECHAM-4: model description and simulation of present-day climate. Max-Planck-Institute for Meteorology Rep. 218, p 90

Saha S et al (2013) The NCEP climate forecast system version 2. J Clim submitted

Roundy PE (2012) Observed structure of convectively coupled waves as a function of equivalent depth: Kelvin waves and the Madden-Julian oscillation. J Atmos Sci 69:2097–2106

Saha S et al (2010) The NCEP climate forecast system reanalysis. Bull Am Meteorol Soc 91:1015–1057

Saji NH, Xie SP, Tam CY (2006) Satellite observations of intense intraseasonal cooling events in the tropical south Indian Ocean. Geophys Res Lett 33:L14704. doi:10.1029/2006GL026525

Senguta D, Goswami BN, Senan R (2001) Coherent intraseasonal oscillation of ocean and atmosphere during the Asian summer monsoon. Geophys Res Lett 28:4127–4130

Shen B-W, Tao W-K, Lin Y-L, Laing A (2012) Genesis of twin tropical cyclones as revealed by a global mesoscale model: the role of mixed-Rossby gravity waves. J Geophys Res 117: D13114. doi:10.1029/2012JD017450

Shinoda T, Hendon H, Glick J (1998) Intraseasonal variability of surface fluxes and sea surface temperature in the tropical western Pacific and Indian Oceans. J Clim 11:1685–1702

Straub KH (2013) MJO initiation in the real-time multi-variate MJO index. J Clim 26:1130–1151

Tiedtke M (1989) A comprehensive mass flux scheme for cumulus parameterization in large-scale models. Mon Weather Rev 117: 1779–1800

Vitart F, Molteni F (2010) Simulation of the Madden-Julian oscillation and its teleconnections in the ECMWF forecast system. Q J Roy Meteorol Soc 136:842–855. doi:10.1002/qj.623

Vitart F, Woolnough S, Balmaseda MA, Tompkins AM (2007) Monthly forecast of the Madden-Julian oscillation using a coupled GCM. Mon Weather Rev 135:2700–2715

Waliser DE (2006) Predictability of tropical intraseasonal variability. In: Palmer T, Hagedorn R (eds) The predictability of weather and climate, 1st edn. Cambridge University Press, Cambridge, pp 275–305

Waliser DE, Lau K-M, Kim J-H (1999) The influence of coupled sea surface temperature on the Madden-Julian oscillation: a model perturbation experiment. J Atmos Sci 56:333–358

Waliser DE, Murtugudde R, Lucas LE (2003) Indo-Pacific Ocean response to atmospheric intraseasonal variability: 1. Austral summer and the Madden-Julian oscillation. J Geophys Res 108(C5):3160. doi:10.1029/2002JC001620

Wang B, Liu F (2011) A model for scale interaction in the Madden-Julian oscillation. J Atmos Sci 68:2524–2536

Wang B, Rui H (1990a) Synoptic climatology of transient tropical intraseasonal convection anomalies: 1975–1985. Meteorol Atmos Phys 44:43–61

Wang B, Rui H (1990b) Dynamics of coupled moist Kelvin-Rossby waves on an equatorial beta-plane. J Atmos Sci 47:397–413

Wang WQ, Seo K-H (2009) The Madden-Julian oscillation in NCEP coupled model simulation. Terr Atmos Ocean Sci 20(5): 713–725. doi:10.3319/TAO.2008.09.17.01(A)

Wang B, Xie X (1997) A model for the boreal summer intraseasonal oscillation. J Atmos Sci 54:72–86

Wang B, Xie X (1998) Coupled modes of the warm pool climate system. Part I: the role of air–sea interaction in maintaining Madden-Julian oscillation. J Clim 11:2116–2135

Wang WQ, Hung M-P, Weaver SJ, Kumar A, Fu XH (2013) MJO prediction in the NCEP climate forecast system version 2. Clim Dyn (in press)

Weaver SJ, Wang WQ, Chen MY, Kumar A (2011) Representation of MJO variability in the NCEP climate forecast system. J Clim 24:4676–4694

Wheeler MC, Hendon HH (2004) An all-season real-time multivariate MJO index: development of an index for monitoring and prediction. Mon Weather Rev 132:1917–1932

Woolnough SJ, Slingo JM, Hoskins BJ (2000) The relationship between convection and sea surface temperature on intraseasonal timescales. J Clim 13:2086–2104

Wu MLC, Schubert S, Kang IS, Waliser DE (2002) Forced and free intraseasonal variability over the south Asian monsoon region simulated by 10 AGCMs. J Clim 15:2862–2880

Zhang CD (2005) Madden-Julian oscillation. Rev Geophys 43:RG2003. doi:10.1029/2004RG000158

Zheng Y, Waliser DE, Stern W, Jones C (2004) The role of coupled sea surface temperatures in the simulation of the tropical intraseasonal oscillation. J Clim 17:4109–4134

Zhu W, Li T, Fu X, Luo J-J (2010) Influence of the Maritime Continent on the boreal summer intraseasonal oscillation. J Meteorol Soc Japan 88:395–407